Int. J. Electrochem. Sci., 15 **(2020)** 11137 – 11149, doi: 10.20964/2020.11.23

International Journal of
ELECTROCHEMICAL
SCIENCE
www.electrochemsci.org

Effect of Electroplating Bath Composition on Corrosion Resistance of Deposited Cobalt Films

Li Jiang, Pengming Long, Fan Qin, Yundan Yu[*], *Shuting Xu, Zerong Yang, Ziyao Guo, Guoying Wei*

College of Materials and Chemistry, China Jiliang University, Hangzhou, China
[*]E-mail: yuyundan@163.com

Received: 6 July 2020 / *Accepted:* 26 August 2020 / *Published:* 30 September 2020

Preparation and corrosion resistance of cobalt films deposited on polycrystalline platinum in different electroplating baths (chloride bath, sulfate bath and chloride-citrate bath) have been studied. Cyclic voltammetry (CV) was used to study the electrodeposition process of cobalt films. Films composition, structure and surface morphology were analyzed by X-ray diffractometer (XRD), atomic force microscope (AFM) and metallographic microscope. Furthermore, the corrosion resistance were measured by potentiodynamic polarization curve and electrochemical impedance spectroscopy (EIS). In different electroplating baths, the shape of cyclic voltammetry curves are similar, where both under-potential deposition behavior and over-potential deposition behavior are presented. The cobalt film obtained from chloride bath is thicker and rougher with acicular shape particles; in sulfate bath, the cobalt grains are spherical shape and the film is smooth with obvious cracks; in chloride-citrate bath, the cobalt grains are seemly much smaller and the film is the smoother and thinner. The component of prepared films in three electroplating baths are mainly cobalt grains with crystal plane of (111), (200) and (220). In 3.5wt.% NaCl solution, the corrosion rate order of deposited cobalt films is $\boldsymbol{v}_{\text{chloride bath}} < \boldsymbol{v}_{\text{sulfate bath}} < \boldsymbol{v}_{\text{chloride-citrate bath}}$.

Keywords: Polycrystalline platinum, Electrodeposition, Cobalt film, Corrosion resistance

1. INTRODUCTION

In recent years, the electrodeposition of cobalt and its alloys has been attracted much more attentions. The cobalt and cobalt alloys possess optimal magnetic properties which can be used in various fields, such as heterogenic catalysts [1], solid oxide fuel cells [2, 3], energy storage systems [4-7], magnetic data carriers [8], constructing spin valve devices and so on. Many preparation methods could be used to fabricate cobalt alloys. The physical methods like molecular beam epitaxy, sputtering, vacuum deposition [6-9], thermal-chemical evaporation [10] and electrodeposition methods [11, 12] are considered as effective ways to prepare cobalt alloys. However, except for these physical methods,

chemical preparation method is also a kind of effective and efficient ways to get cobalt alloys with good properties. It is well known that electroplating is also considered as a good method to make metal alloys due to its positive advantages. Plating technology is cheap, stable and easy to operate. It is possible to change the properties of metal alloys prepared by plating technology by changing the electrochemistry parameters.[13].

Cobalt has been electrodeposited mainly onto carbon, gold, platinum, palladium, stainless steel, nickel and copper substrates [14-16]. Various solutions were used for cobalt electrodeposition, but among them simple salt acidic chloride [4, 7], sulfate [9-11] and chloride-sulfate [12] baths were dominating. Less attention was paid on the metal deposition from complex salts electrolytes, e.g. ammoniacal [13, 14], citrate [15], gluconate [16] or glycine [17] systems.

According to many reports and researches, the physical performance and thermal stability of cobalt alloys are relevant to the kinetics and mechanism of the cobalt plating process.[10-15]. Therefore, it is essential to research the effect of electrochemical parameters such as potentials, plating time, temperature, current density on the structure, morphology and performance of cobalt alloys. [16-22].

In spite of some research on cobalt electrodeposition, there is limited study about the effects of bath composition on the characteristics and properties of cobalt films. This paper shows comparative studies of the electrolytes (chloride bath, sulfate bath and chloride-citrate bath), since the speciation and buffering properties of the solution can affect the nucleation stage, morphology and structure of the deposits. The cobalt electrodeposition onto polycrystalline platinum was studied using cyclic voltammetry (CV) to gain a deeper insight into the cobalt under-potential deposition and over-potential deposition process. Films composition, structure and surface morphology were analyzed by XRD, AFM and metallographic microscope. Furthermore, corrosion resistance of cobalt films electrodeposited in different baths were also investigate.

2. EXPERIMENTAL

2.1 Pretreatment of polycrystalline platinum electrode

The polycrystalline platinum plate (high purity of 99.99 %) with dimension of 20.0 mm × 20.0 mm ×1.0 mm was used as the working electrode. Its surface was treated by electrochemical polishing technology [23] and the pretreatment procedures are as follows: (1) the electrode was ultrasonically cleaned in ethanol and acetone at 25°C for 10 min, then rinsed with deionized water; (2) transfered the electrode to 0.5 mol/L H_2SO_4 solution for electrochemical polishing using cyclic voltammetry technology. The scanning rate was 100 mV/s and the scan potential range was from 0.77 V to -0.65 V (vs. MSE, avoiding the interference of chloride ion to experiment). Until the cyclic voltammetry curves were stabilized, the electrochemical polishing experiment stopped; (3) rinsed the electrode with deionized water and blow-dry with nitrogen. In order to better compare with the results of other researchers, potentials values in this paper were all recalculated relative to saturated calomel electrode (SCE).

2.2 Bath preparation and electrodeposition condition

Three-electrode system was adopted in the experiment, where polycrystalline platinum plate (purity 99.99%) was the working electrode, a platinum foil (purity 99.90%) as a counter electrode and a saturated calomel electrode (SCE, in saturated KCl solution) as the reference electrode. The electroplating bath composition and electrodeposition conditions are presented in Table 1. The pH value was adjusted by 1.0 mol/L NaOH and/ or 1.0 mol/L H_2SO_4 solution. In order to determine the optimum deposition potential of cobalt film, cyclic voltammetry in different baths were performed with scan rate of 20 $mV \cdot s^{-1}$ at the potential range from 0.600 V to -0.980 V.

Table 1. Electroplating baths composition and electrodeposition conditions

	Chloride bath	**Sulphate bath**	**Chloride-citrate bath**
$CoCl_2 \cdot 6H_2O$ / $(mol \cdot L^{-1})$	0.01	-	0.01
NH_4Cl / $(mol \cdot L^{-1})$	1.00	-	1.00
pH	8.00	8.00	8.00
$CoSO_4 \cdot 7H_2O$ / $(mol \cdot L^{-1})$	-	0.01	-
$(NH_4)_2SO_4$ / $(mol \cdot L^{-1})$	-	1.00	-
$Na_3C_6H_5O_7 \cdot 2H_2O$ / $(mol \cdot L^{-1})$	-	-	0.01
Deposition potential / V	-1.00	-1.00	-1.00
Deposition time / h	1.00	1.00	1.00

2.3 Morphology and structure analysis

X-ray diffraction (XPert Philips PW1830) was adopted to analyze the structure of deposited cobalt films, where Cu Kα radiation was used as an incident beam (40kV, 150mA). Scanning electron microscopy (SEM, Hitachis-4800) was used to observe the surface morphology. Moreover, atomic force microscope (AFM, D3100) and metallographic microscope (Smart zoom 5, Carl Zeiss) were used to characterize the roughness and thickness of each sample.

2.4 Corrosion resistance analysis

The corrosion resistance of the deposited cobalt films was evaluated by potentiodynamic polarization measurement and electrochemical impedance spectroscopy (EIS). The test was performed on electrochemical working station ((PARSTAT®2273) with a three-electrode cell. The polycrystalline platinum deposited with cobalt films were treated as the working electrode; the counter electrode and reference electrode were the same with section 2.2. The test environment was 3.5 wt.% NaCl solution at 25°C. The test range of the potentiodynamic polarization curve was [E_{ocp} -300mV, E_{ocp}+300mV] with the scan rate of 1.0m $V \cdot s^{-1}$. The corrosion current i_{corr} was calculated by tafel linear extrapolation method. EIS was carried out at a range of 10 mHz ~100 kHz with a 5mV perturbation signal at the corrosion potential. The results of EIS were used to simulate the equivalent electrical

circuit of electrodeposition process using *Z*-view software. Duplicate experiments were conducted to ensure the reliability and reproducibility of the measurements.

3. RESULTS AND DISCUSSION

3.1 Pretreatment of polycrystalline platinum electrodes

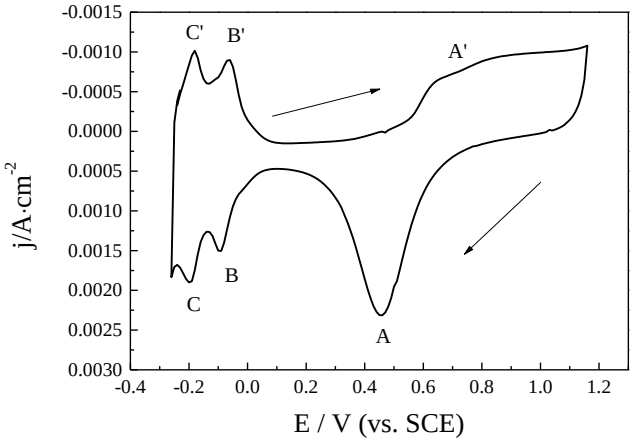

Figure 1. Cyclic voltammetry curve of polycrystalline platinum electrode in 0.5 M H_2SO_4 solution with scan rate of 20 $mV \cdot s^{-1}$ at the potential between 1.1 V and -0.300 V.

The surface of polycrystalline platinum electrode was treated by electrochemical polishing technology. Fig. 1 shows the CV curve of this electrode in 0.5 M H_2SO_4 solution. According to the evolution of CV curve, it can be divided into three potential regions: (1) the platinum redox region (from 0.45 V to 1.2 V), where peak A (0.46 V) is the platinum reduction peak and peak A' is the platinum oxidation peak; (2) the hydrogen adsorption and desorption region (from –0.25 V to 0.1 V), where peak B (–0.08 V) and peak C (–0.19 V) are hydrogen desorption peaks, and peak B' (–0.05 V) and peak C' (–0.18 V) are hydrogen adsorption peaks; (3) the double electric layer region (from 0.1 V to 0.45 V). This characteristics are consistent with those reported in relevant literature [24].

Furthermore, the H adsorption area (H_{ad}) and needed electricity $Q_{H,1ML}$ on polycrystalline platinum electrode can also be calculated from the CV curve. The formula for active area calculation of electrode is shown as following:

$$A = Q_{H,1ML} / q_H^S = Q_{H,1ML} / 210\ \mu C/cm^2 \qquad (1)$$

Where, $Q_{H,1ML}$ refers to the adsorption and desorption amount of 1 ML (1 monolayer) H, and q_H^S refers to the electric density of H atom adsorbed by monolayer on polycrystalline platinum at a certain potential, with a size of 210 $\mu C/cm^2$. In this experiment, the calculated active area of polycrystalline platinum electrode is about 1.500 cm^2.

3.2 Electrodeposition of cobalt films in different baths

CV curves of cobalt films electrodeposited on polycrystalline platinum in different electrolyte baths are shown in Fig.2. In chloride bath (Fig. 2a), the potentials of peak A (appear at -0.37 V) and peak B (appear at -0.65 V) are more positive than -0.741 V, indicating the under-potential deposition behavior of Cobalt. Peak A is caused by the supporting electrolyte, and peak B may be associated with Co^{2+} reduction process [25]. The cobalt over-potential deposition initiates at -0.741 V and peak C (appear at -0.90 V) is the distinct cobalt over-potential deposition peak. When reverse scan, peak D, E and F appear at -0.80 V, -0.55 V and 0.32 V, respectively. Peak D may be related to the formation of hydrogen-rich Co phase; peak E is the dissolution peak of cobalt over-potential deposition, and peak F is the dissolution peak of Co under-potential deposition [26]. It is reported that the cobalt nucleation rate is faster in alkaline baths, which associated with the competition for the active sites on the surface by H ions with the Co cations [17, 20].

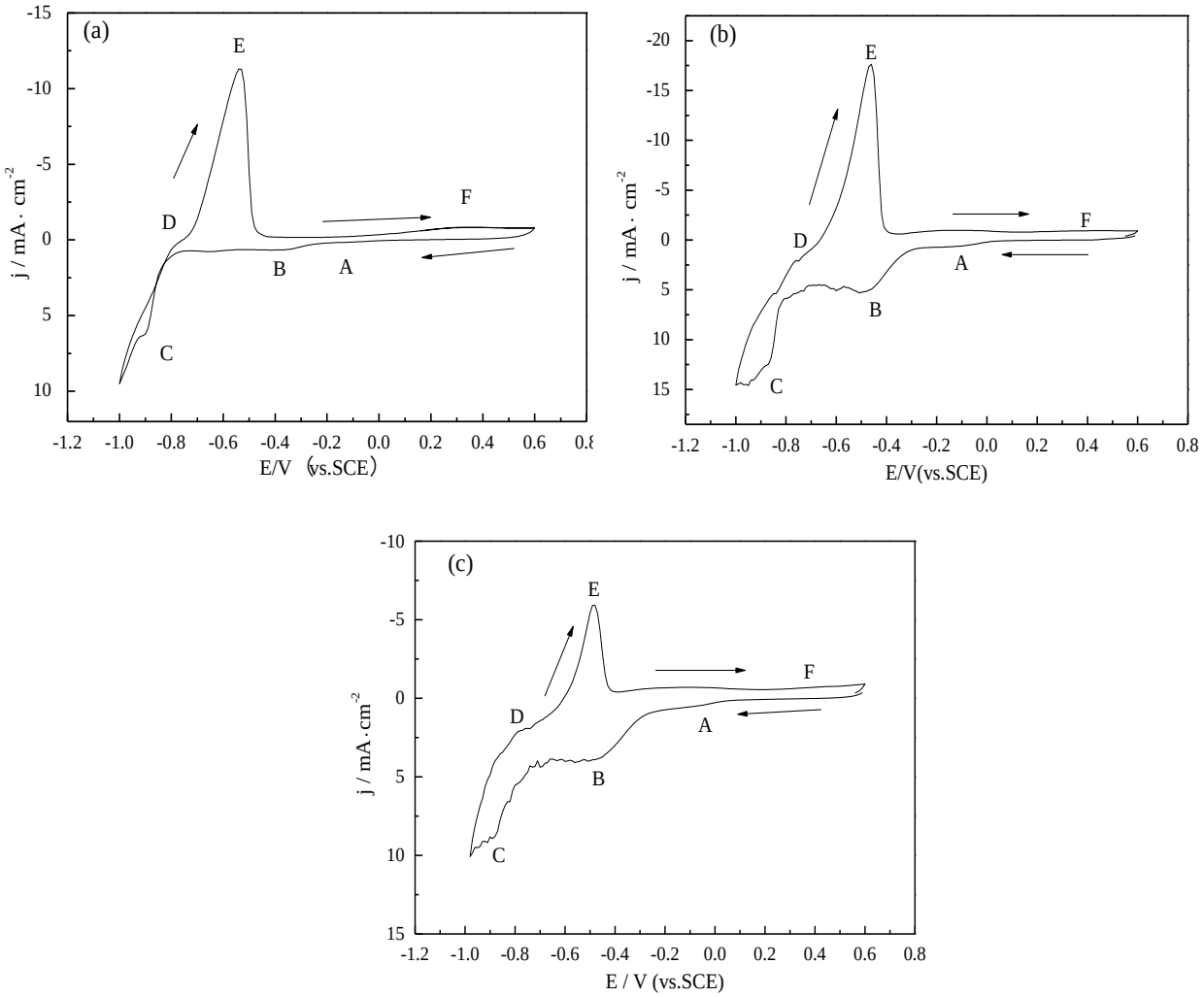

Figure 2. Cyclic voltammetry curves of cobalt films deposited on polycrystalline platinum electrode in different electroplating baths with scan rate of 20 $mV \cdot s^{-1}$ at the potential between 0.6 V and -1.0 V: (a) chloride bath; (b) sulfate bath; (c) chloride-citrate bath;

The shapes of cyclic voltammetry curves in Fig. 2a, Fig. 2b and Fig. 2c are similar. However, the current density of peak B, peak C and peak E in Fig. 2b are higher than that in Fig. 2a. It mainly due to the concentration of NH_4^+ in sulfate bath is higher, which is important to the electrical conductivity of solution [27]. In chloride bath and sulfate bath, free chloride and sulfate ions play main roles as they are known to adsorb on cathode and participate in the solution buffering in different way. Ions adsorbed on the cathode surface inhibit charge transfer across the metal-electrolyte interface, hence they can increase over-potential for the cathodic reaction. Moreover, better buffering properties of the sulfate baths for the base addition improve the electrodeposition of cobalt by protecting against intensive hydrogen coevolution and formation of residual hydroxide species. In turn, weak adsorption of chloride ions does not disturb reduction of cobalt ions giving lower metal cathodic over-potentials. However, smaller buffering of the chloride solution provides favorable conditions for hydrogen coevolution with lower rate of reaction, resulting lower current efficiency for pure metal electrodeposition at more electronegative deposition potentials [28]. In sulfate bath, it was also found that the cathodic process was seriously affected by sulfate ions, changes in the promotion of the hydrogen evolution reaction and the improvement of film surface morphology [29]. Meanwhile, in the chloride-citrate bath, strong adsorption of sodium citrate on the cathode inhibited hydrogen evolution, favored fast metal nucleation and deposition of fine grained coatings, the presence of chloride ions and low citrate ions concentration resulted in the formation of hydroxide species [30]. The chloride-citrate bath with complex salt have better buffering effects and allow obtaining highly adherent and lustrous films [17].

3.3 Surface analysis of deposited cobalt films

Fig. 3 shows the 2D surface morphology and thickness of the deposited cobalt films on polycrystalline platinum electrode in different electroplating baths using SEM and metallographic microscope. The morphology of nanocrystals mainly depends on the relative growth rate of each crystal surface during crystal growth [30]. The rate of crystal surface growth is controlled by the addition of surfactants or anions (such as Cl^-) with strong adsorption on a certain crystal surface. Citrate and halogen anions may be adsorbed on the surface of platinum nanocrystals in the electrodeposition system. The cobalt particles obtained from chloride bath are uniformly arranged with acicular shape. The film thickness is about 8.24μm (shown in Fig.3a). Fig. 3(b) shows that the film obtained from sulfate bath is smoother, but has obvious cracks. The film thickness is about 6.57μm, indicating that the deposition rate was slower than that in chloride bath.

Many cracks could be found on the surface of cobalt film which is common and reported by many researchers.[20, 28, 31]. It is found out that the tensile stress in the main reason that causes cracks on the film surface. There are mainly four types of tensile stress: interfacial stress between the film and the substrate, crystallographic texture and grain size, coalescence and stress evolution during the film growth and hydrogen adsorption/ desorption [32]. However, the tensile stress associated with cobalt films is not very large due to good adhesion between films and substrate. Especially, in the condition of chloride-citrate bath, the film surface quality is improved because of finer grains with

only 5.79 μm thickness. (Fig.3c). The citrate ions in the bath could be adsorbed on the surface of cathode to hinder the diffusion process of ad-ions resulting in the decrease of grain growth rate which contribute directly to finer crystallites. [30, 31].

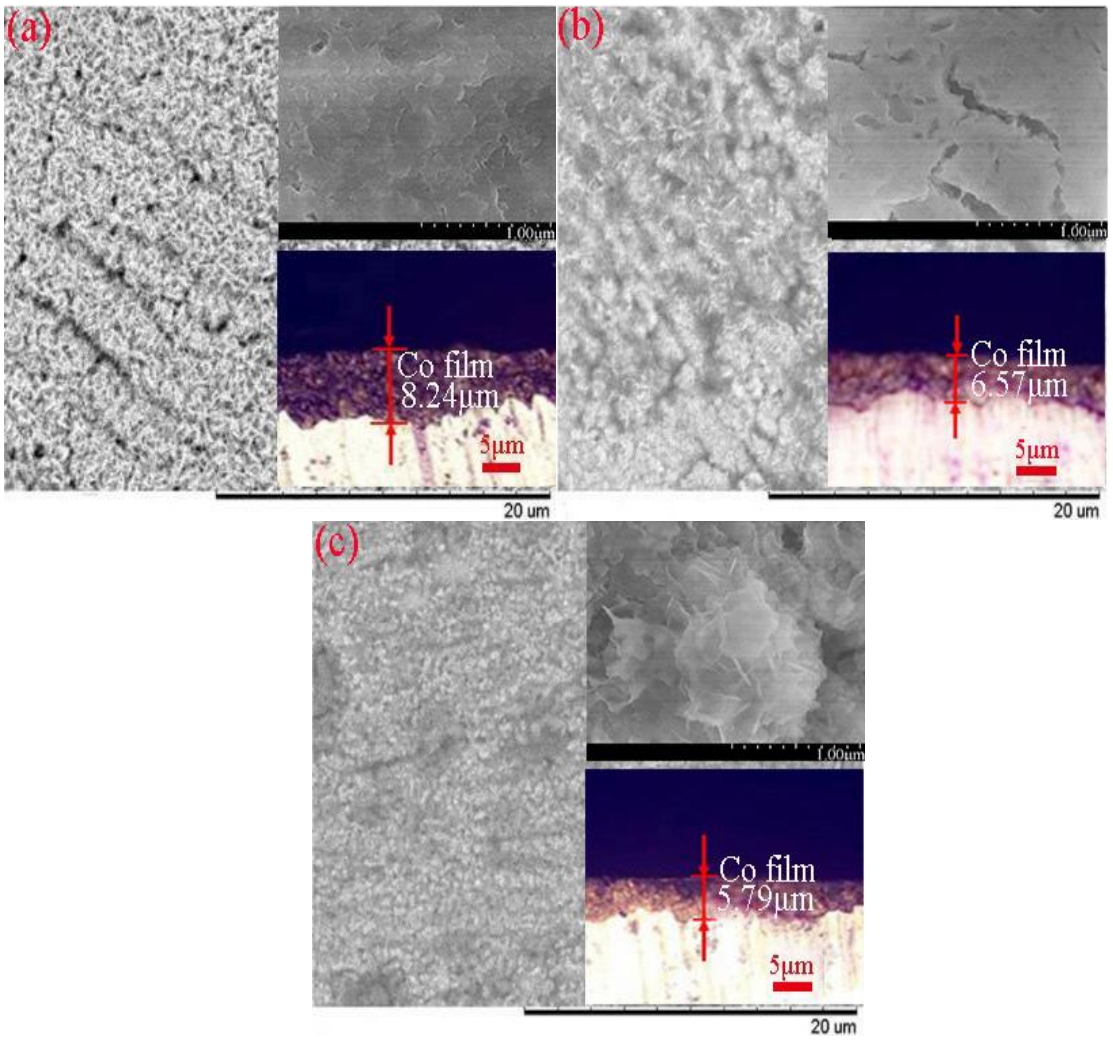

Figure 3. 2D surface morphology and thickness of deposited cobalt films on polycrystalline platinum electrodes in different electroplating baths: (a) chloride bath; (b) sulfate bath; (c) chloride-citrate bath

Fig. 4 shows the 3D surface morphology and roughness of deposited cobalt films on polycrystalline platinum electrodes in chloride bath, sulfate bath and chloride-citrate bath using AFM. In chloride bath, the grains of film are needle shape and densely packed (shown in Fig.3a) with the surface roughness R_a 78.6 nm and R_q 99.7 nm. In sulfate bath, the grains of film are spherical shape (shown in Fig.3b) with the surface roughness R_a 47.0 nm and R_q 58.9 nm, which is smoother and flatter than that deposited from the chloride bath. While in chloride-citrate bath, the grains of film are seemly the smallest and finest, with surface roughness R_a 18.0 nm and R_q 23.7 nm. According to the ions adsorption on cathode and solution buffering explanation in section 3.2, the obtained experimental results confirm this theoretical prediction [33].

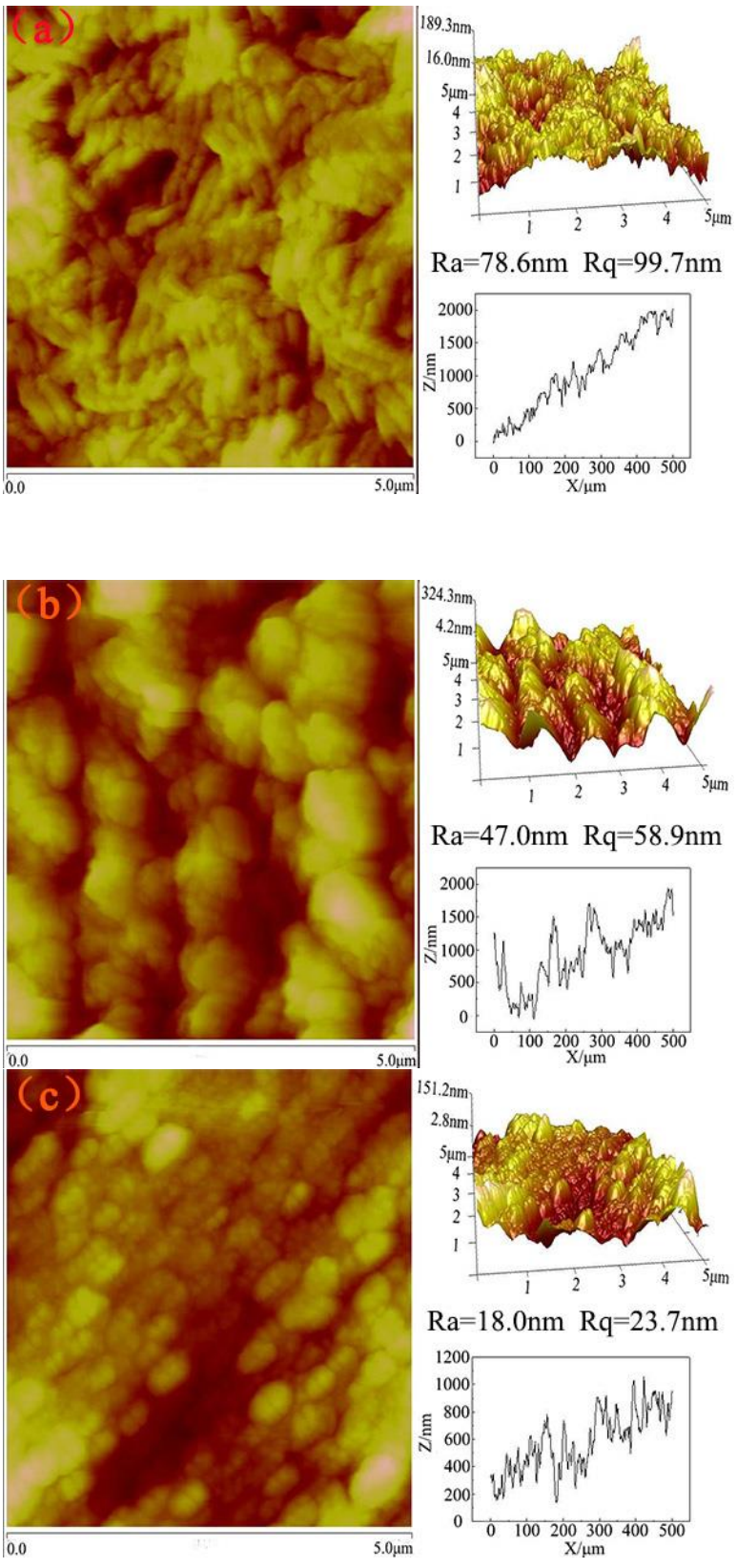

Figure 4. 3D surface morphology and roughness of deposited cobalt films on polycrystalline platinum electrodes in different electroplating baths: (a) chloride bath; (b) sulfate bath; (c) chloride-citrate bath

3.4 Composition of deposited cobalt films

Structural analysis of deposited cobalt films on polycrystalline platinum electrodes at different electroplating baths were performed by XRD (Fig.5). The component of prepared films are mainly cobalt grains and the crystallographic orientations of cobalt grains are presented at 2θ≈44.2°, 51.2° and 75.8°, which corresponds to crystal plane of (111), (200) and (220). In different baths, the adsorption layer formed by chloride ions, sulfate ions and citrate ions may have different structure and stability on different crystal surfaces of cobalt, which results in the difference of crystal surface growth rate and the different morphology [34]. In chloride baths, the diffraction peak height ratio of cobalt crystal plane (111):(200):(220) is 0.886:0.561:1; in sulfate bath, the diffraction peak ratio of cobalt crystal plane (111):(200):(220) is 1.728:0.596:1, where grains with crystal plane of (111) and (200) increase; and in chloride-citrate bath, the diffraction peak ratio of cobalt crystal plane (111):(200):(220) is 1.596:0.716:1. It indicates that the addition of citrate in chloride bath (shown in Table 1) will change the preferred orientation of cobalt grain growth, and grains with crystal plane of (111) and (200) increase.

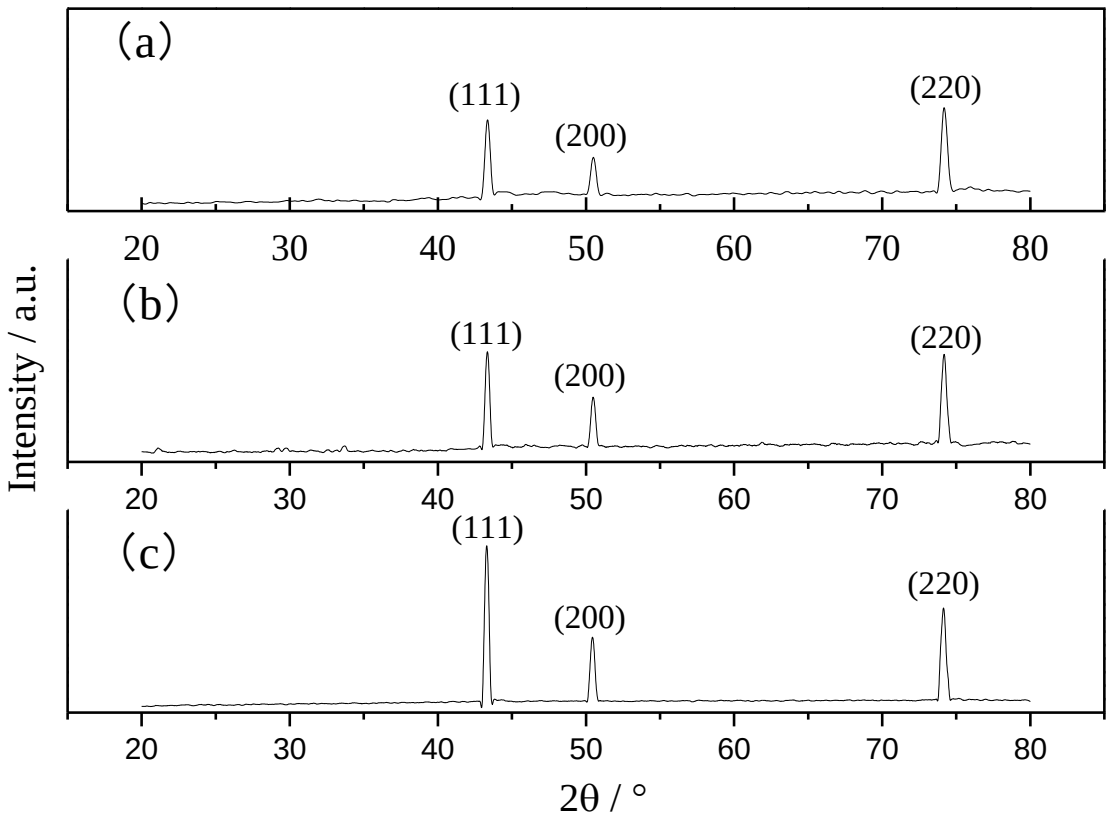

Figure 5. X-ray diffraction pattern of the deposited cobalt films on polycrystalline platinum electrodes in different electroplating baths: (a) chloride bath; (b) sulfate bath; (c) chloride-citrate bath

3.5 Corrosion resistance of deposited cobalt films

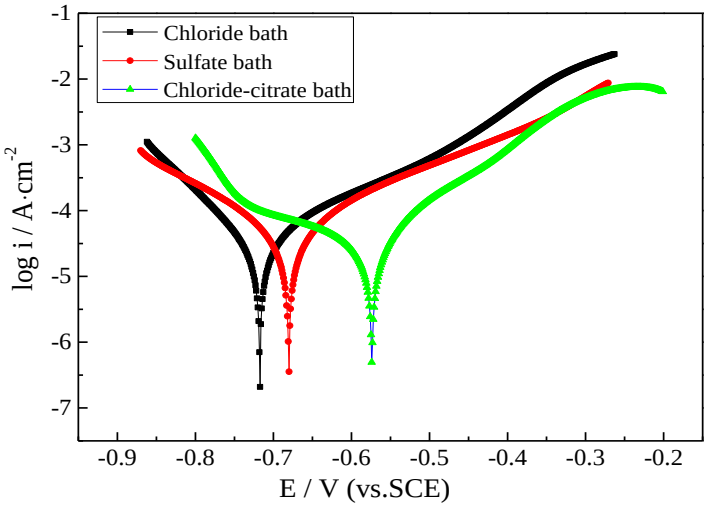

Figure 6. Potentiodynamic polarization curves of deposited cobalt films on polycrystalline platinum electrode in 3.5 wt.% NaCl solution with scanning rate of 1 mV/s

Table 2. Electrochemical corrosion data corresponding to potentiodynamic polarization curves of deposited cobalt films on polycrystalline platinum electrode in 3.5 wt.% NaCl solution

Sample	E_{corr}/V	I_{corr}/(10^{-5}A·cm^{-2})
Chloride bath	-0.723	1.18
Sulfate bath	-0.695	2.31
Chloride-citrate bath	-0.587	3.10

Fig.6 shows the potentiodynamic polarization curves of deposited cobalt film samples in 3.5 wt.% NaCl solution. Table 2 shows electrochemical corrosion data corresponding to the potentiodynamic polarization curves. In the corrosion system, the electrochemical reaction process is controlled by the oxygen diffusion process. In the presence of aggressive ions, especially Cl^-, pitting corrosion takes place depending on the chloride concentration and the physico-chemical characteristics of the passive film [16-19]. Compared the three electroplating baths, the corrosion potential order of deposited cobalt films is $E_{\text{corr-chloride bath}} < E_{\text{corr-sulfate bath}} < E_{\text{corr-(chloride-citrate bath)}}$; and the corrosion current density order of deposited cobalt films is $I_{\text{corr-chloride bath}} < I_{\text{corr-sulfate bath}} < I_{\text{corr-(chloride-citrate bath)}}$.

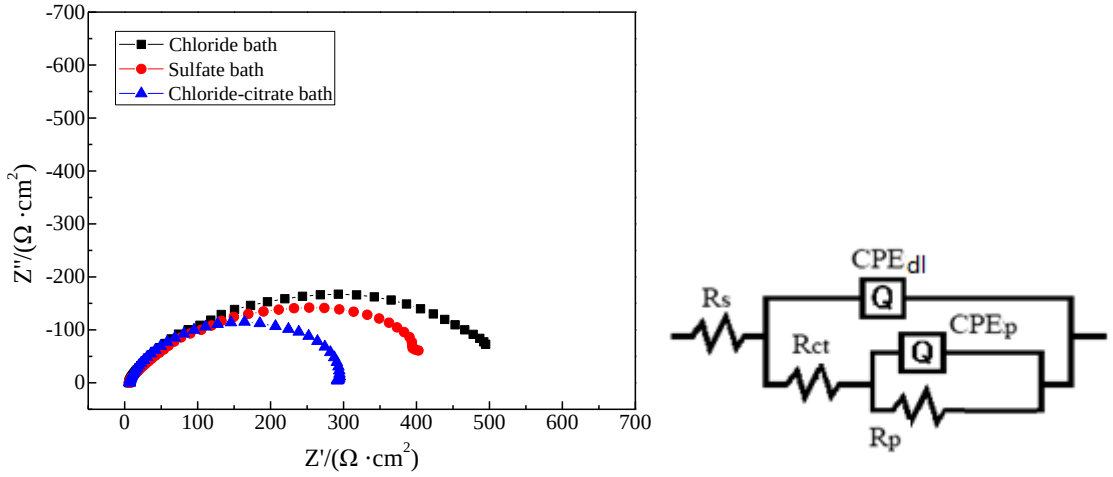

(a) (b)

Figure 7. Nyquist plots (a) and equivalent circuit (b) for deposited cobalt films in 3.5wt.% NaCl solution at a range of 10 mHz ~100 kHz with a 5mV perturbation signal

Table 3. Values of the elements in the equivalent circuit of deposited cobalt films in 3.5wt.% NaCl solution

Sample	R_s/ (Ω·cm²)	CPE_{d1}/ (μF·cm²)	n_1	R_{ct}/ (Ω·cm²)	CPE_p / (μF·cm²)	n_2	R_p/ (Ω·cm²)
Chloride bath	5.973	36.4	0.933	71.34	118.1	0.589	436.7
Sulfate bath	6.025	30.65	0.931	71.21	132.1	0.657	369.2
Chloride-citrate bath	6.081	37.79	0.945	71.15	174.8	0.790	299.5

EIS experiments were carried out to explore the mechanism of corrosion resistance. The Nyquist plots and equivalent circuits of EIS tests in 3.5wt.% NaCl solution are shown in Fig.7. The frequency dependence of dispersion capacitive behavior is often described by employing a constant phase element (*CPE*) [29]. Fig. 7 is employed to fit EIS experiments data. R_{ct} and R_s stand for the charge transfer and the electrolyte resistance respectively. R_p is considered as the Faradaic resistance of the cobalt film. The definition of the impedance for *CPE* can be described as followings:

$$Z_{CPE} = [\,(j\omega)^n \times T]^{-1} \qquad (2)$$

where j is $(-1)^{1/2}$; ω and T are the angular frequency and the double-layer capacitance quantity, n is an exponent affected by the phase angle. The EIS data were fitted and calculated by the Armstrong equivalent circuit which had been modified. The fitting results are listed in Table 2. Compared the cobalt film prepared in chloride bath (shown in Fig7a), cobalt film prepared in the sulfate bath has smaller diameter of semicircle; and film prepared in chloride-citrate bath has the smallest diameter of semicircle. The diameter of semicircle decrease indicates that the sum of charge transfer resistance R_{ct} and the Faradaic resistance R_p of the cobalt film decrease. This conclusion has been confirmed , according to Table 3: $(R_p+R_{ct})_{\text{Chloride bath}} > (R_p+R_{ct})_{\text{Sulfate bath}} > (R_p+R_{ct})_{\text{Chloride-citrate bath}}$. The corrosion rate $\boldsymbol{v}$ can be representation by $1/(R_p+R_{ct})$ [35], and the corrosion rate order can be deduce: $\boldsymbol{v}_{\text{chloride bath}} <$

$v_{\text{sulfate bath}} < v_{\text{chloride-citrate bath}}$. This results is the same with that obtained from the analysis of potentiodynamic polarization curves.

4. CONCLUSIONS

The electrodeposition process and corrosion resistance of cobalt films on polycrystalline platinum electrode in different electroplating baths have been investigated. The results are drawn as follows:

(1) In different electroplating baths, the shape of cyclic voltammetry curves are similar. The potentials of peak A and peak B indicate the under-potential deposition behavior of cobalt; peak C is the distinct cobalt over-potential deposition peak. When reverse scan, peak D may be related to the formation of hydrogen-rich cobalt phase; peak E is the dissolution peak of cobalt over-potential deposition, and peak F is the dissolution peak of cobalt under-potential deposition.

(2)The cobalt particles obtained from chloride bath are uniformly arranged with acicular shape; in sulfate bath, the cobalt grains of film are spherical shape, with smooth film surface and some obvious cracks. In chloride-citrate bath, the cobalt grains of film are the smaller and finer, and the film is the thinner. (3)The component of deposited films are mainly cobalt grains and the crystallographic orientations of cobalt grains are presented at $2\theta \approx 44.2°$, 51.2° and 75.8°, which corresponds to cobalt crystal plane of (111), (200) and (220). In sulfate bath and chloride-citrate bath, cobalt grains with crystal plane of (111) and (200) increase.

(4) In 3.5 wt.% NaCl solution, the electrochemical reaction process is controlled by the oxygen diffusion process. The corrosion rate order of deposited cobalt films in different electroplating baths is $I_{\text{corr-chloride bath}} < I_{\text{corr-sulfate bath}} < I_{\text{corr-(chloride-citrate bath)}}$.

ACKNOWLEDGEMENT
This research was supported by the Zhejiang Provincial Natural Science Foundation of China (No. LY17B030006).

References

1. L. F. Sallum, E. R. Gonzalez and A. Mota-Lima, *Electrochem. Commun.*, 90(2018)26.
2. C. H. Chen, A. Halford, M. Walker, C. Brennan and P. Rodriguez, *J. Electroanal. Chem.*, 816(2018) 138.
3. M. D. Detwiler,C. A. Milligan,D. Y. Zemlyanov, W. N. Delgass and F. H. Ribeiro, *Surf. Sci.*, 648 (2016)220.
4. J. M. Falkowski, N. M. Concannon, B. Yan and Y. Surendranath, *J. Am. Chem. Soc.*,137(2015) 7978.
5. Y. Furuya, T. Mashio, A. Ohma and G. Jerkiewicz, *Electrocatalysis*, 6(2015)109.
6. M. Fayette, A. Nelson and R. D. Robinson, *J. Mater. Chem. A*, 3(2015)187.
7. M. Quinet, F. Lallemand, L. Ricq, J.Y. Hihn and P. Delobelle, *Surf. Coat. Tech.*, 204(2010)3108.
8. O. V. Cherstiouk, A. N. Simonov and G. A. Tsirlina, *Electrocatalysis*, 3(2012)230.

9. L. F. Sallum, E. R.Gonzalez and J. M. Feliu, *Electrochem. Commun.*, 72(2016)83.
10. P. Sadeghi, K. Dunphy, C. Punckt and H. H. Rotermund, *J. Phys. Chem. C.*, 116(2012)4686.
11. D. Grujicic and B. Pesic, *Electrochim. Acta*, 49 (2004)4719.
12. M. Doulache, B. Saidat and M. Trari, *J. Anal. Chem.*, 72(2017)333.
13. M. Delgosha, S. Salehi, L. U. borujeni and S. Sharifi, *Opt.*, 3(2014)15.
14. P. Boguslaw, P. Grazyna and M. Tomasz, *Pol. J. Chem. Technol.*, 17(2015)126.
15. P. Y. Olu, T. Ohnishi, Y. Ayato, D. Mochizuki and W. Sugimoto, *Electrochem. Commun.*, 71(2016) 69.
16. V. Babenko, A. T. Murdock, A. A. Koo´s, J. Britton, A. Crossley, P. Holdway, J. Moffat, J. Huang, J. A. Alexander-Webber, R. J. Nicholas and N. Grobert, *Nat. Commun.*,7(2015)1.
17. M. Potgieter, J. Parrondo, V. K. Ramani and R. J. Kriek, *Electrocatalysis*, 7(2016)50.
18. N. S. Georgescu, D. A. Scherson and A. J. Jebaraj, *J. Phys. Chem.*, 120(2016)16090.
19. P. Allongue, L. Cagnon, C. Gomes, A. Gundel and V. Costa, *Surf. Sci.*, 557(2004)41.
20. Y. Kuo, W. Liao and S. L.Yau, *Langmuir*, 30(2014)13890.
21. L. H. Mendoza-Huizar and C. H. Rios-Reyes, *Cent. Eur. J. Chem.*, 11(2013)1381.
22. A. Krause, M. Uhlemann, A. Gebert and L. Schultz, *J. Solid State Electrochem.*, 11(2007)679.
23. L.H. Mendoza-Huizar and C. H. Rios-Reyes, *J. Solid State Electrochem.*, 15(2011)737.
24. M. C.Santos, D. W. Miwa and S. A. S. Machado, *Electrochem. Commun.*, 2(2000)692.
25. W. Szmaja, W. Kozłowski, K. Polan′ski, J. Balcerski, M. Cichomski, J. Grobelny, M. Zielinski and E. Miekos, *Chem. Phys. Lett.*, 542(2012)117.
26. L. H. Mendoza-Huizar and C. H.Rios-Reyes, *J. Solid State Electr.*, 16(2012)2899.
27. P. F. Wu, J. B. Shi and Y. C. Chang, *Cryst. Res. Technol.*, 49(2014)873.
28. E. Rudnik, *J. Electroanal. Chem.*, 726(2014)97.
29. E. Rudnika and N. Dashbold, *Russ. J. Elecrochem.*, 55(2019)1305.
30. E. Rudnik. *J. Electroanal. Chem.*, 741(2015)20.
31. B.H. Lu, H.J. Shi, D.S Li, B. Wu, Y. Liu, X.W. Fan and Y. Z. Tang, *Electroplat. & Finishing*, 28 (2019)1324.
32. W. Kozłowski , I. Piwoński, W. Szmaja, M. Zieliński, W. Kozłowski, I. Piwoński, W. Szmaja and M. Zieliński, *J. Electroanal. Chem.*, 769(2016)42.
33. S.S.A. El Rehim, M.A.M. Ibrahim and M.M. Dankeria, *J. Appl. Electrochem.*, 32(2002)1019.
34. Y.Y. Liu, P. Diao and M. Xiang, *Acta Chim. Sinica*, 69(2011)1301.
35. P. Jiao, N. Duan, C. Zhang, F. Xu, G. Chen, J. Li and L. Jiang, *Int. J. Hydrog. Energy*, 41(2016) 17793.